Green Chemistry

PAPER

View Article Online
View Journal | View Issue

Cite this: *Green Chem.*, 2017, **19**, 3927

Immobilization engineering – How to design advanced sol–gel systems for biocatalysis?†

Diána Weiser,‡[a,b,c] Flóra Nagy,‡[a] Gergely Bánóczi,[a] Márk Oláh,[a] Attila Farkas,[a] András Szilágyi,[d] Krisztina László,[d] Ákos Gellért,[e] György Marosi,[a] Sándor Kemény[f] and László Poppe *[a,b,g]

An immobilization engineering approach using bioinformatics and experimental design tools was applied to improve the sol–gel enzyme entrapment methodology. This strategy was used for the immobilization of lipase B from *Candida antarctica* (CaLB), a versatile enzyme widely used even on the industrial scale. The optimized entrapment of CaLB in sol–gel matrices is reported by the response-surface methodology enabling efficient process development. The immobilized CaLBs characterized by functional efficiency and enhanced recovery provided economical and green options for flow chemistry. Various ternary mixtures of sol–gel precursors allowed the creation of tailored entrapment matrices best suited for the enzyme and its targeted substrate. The sol–gel-entrapped forms of CaLB were excellent biocatalysts in the kinetic resolutions of secondary alcohols and secondary amines with aromatic or aliphatic substituents both in batch and continuous-flow biotransformations.

Received 23rd March 2017,
Accepted 19th July 2017

DOI: 10.1039/c7gc00896a

rsc.li/greenchem

Introduction

Biocatalysis, as an efficient and green tool for modern organic synthesis, is becoming increasingly important due to its high activity, high chemo-, regio-, and/or stereoselectivity under mild reaction conditions, and limited by-product formation.[1] Biocatalysts permit the transformation of multifunctional molecules with functional group selectivity, generally obviating functional group activation, protection, and deprotection steps required in traditional organic syntheses.[2] The advantages of reducing the number of synthetic steps – such as reduction of waste and hazards, improvement of the overall yield and cutting of costs – are obvious.

In spite of their benefits, the use of chemo/enzymatic routes is limited because the relevant enzymes are often commercially not available, and the development of robust biocatalysts suitable for industrial processes is slow and expensive.[3]

Modern methods of synthetic biology allow unprecedented potential for engineering proteins possessing novel functions.[4]

These methods can help to fill deficiencies of the biocatalysis toolbox at the molecular level. Moreover, both natural and engineered enzymes are "naked" proteins which might be further decorated to endow them with additional properties to extend their scope of applications in various reactions in a green manner.

Lipases represent one of the most frequently used enzyme classes due to their ability to catalyze a wide range of reactions – such as esterification, transesterification, aminolysis, polymerization – in a mild and selective manner without external cofactors.[5] Lipase-catalyzed reactions cover a wide range of applications ranging from producing biofuels,[6,7] fragrances,[8] and food ingredients[9] to the enantioselective synthesis of enantiopure active pharmaceutical ingredients (API).[10] Kinetic resolution (KR) of racemic mixtures is one of the most important applications of lipases. Lipase B from *Candida antarctica* (CaLB) is one of the most widely used biocatalysts[11,12] lending itself as an ideal target for immobilization engineering.

Large scale applications of enzymes as green biocatalysts are only viable if economically sound. In this respect, stability, storability, and reusability are of prime importance.[13] For improving on these features, immobilization is an adequate solution.[14] Although the major criteria for process assessment

[a]*Department of Organic Chemistry and Technology, Budapest University of Technology and Economics, Műegyetem rkp. 3, H-1111 Budapest, Hungary. E-mail: poppe@mail.bme.hu*
[b]*SynBiocat LLC, Szilasliget u 3, H-1072 Budapest, Hungary*
[c]*Fermentia Ltd, Berlini út 47-49, H-1049 Budapest, Hungary*
[d]*Department of Physical Chemistry and Materials Science, Budapest University of Technology and Economics, Műegyetem rkp. 3, H-1111 Budapest, Hungary*
[e]*Agricultural Institute, Centre of Agricultural Research, Hungarian Academy of Sciences, Brunszvik u. 2, H-2462 Martonvásár, Hungary*
[f]*Department of Chemical and Environmental Process Engineering, Budapest University of Technology and Economics, Műegyetem rkp. 3, H-1111 Budapest, Hungary*
[g]*Biocatalysis and Biotransformation Research Center, Babeş-Bolyai University of Cluj-Napoca, Arany János str. 11, RO-400028 Cluj-Napoca, Romania*
†Electronic supplementary information (ESI) available. See DOI: 10.1039/c7gc00896a
‡These authors contributed equally.

– high activity, high stability, and low costs – are always similar,[15] there is no universal method of enzyme immobilization. The optimal method of immobilization depends on the enzyme, on the substrate, and on the desired process.[14,15]

The sol–gel encapsulation involving the formation of a silica matrix with the biomolecule present during polymerization turned out to be a versatile method.[16] The process proved to be an easy and effective way to immobilize many different types of enzymes such as lipases.[7,17] Sol–gel immobilization often enhances the thermostability, mechanical resistance, solvent tolerance and storage stability of enzymes.[17]

The sol–gel process is initiated by the hydrolysis of tetraalkoxysilanes [$Si(OR)_4$] followed by polycondensation in the presence of the enzyme to be trapped producing a dense silica gel polymeric network. Hydrolysis and condensation of the silane precursors are catalyzed by weak acids or bases, promoting cross-linking and simultaneous encapsulation of the protein by physical forces.[17] Mass transfer limitations of the substrate influx and product efflux were found to be a challenging disadvantage while entrapping enzymes within an inert matrix.[14a,d] The substrate-active site flux was found to depend on the pore size and particle morphology.[18] The significant activity enhancement of the immobilized lipases may be brought about when $Si(OR)_4$ is applied in an admixture with hydrophobic silanes [$R'Si(OR)_3$ or $R'_2Si(OR)_2$] bearing various substituents (R′ being an alkyl or aryl group).[19] By mixing of $Si(OR)_4$ with more hydrophobic silanes of type $R'Si(OR)_3$ or $R'R''Si(OR)_2$, the hydrophobicity of the matrix can be fine-tuned resulting in an increase of lipase activity. The high variability of the precursors and entrapment conditions make the sol–gel technology especially suitable to control the catalytic properties of the immobilized enzymes.[17,19] Reports on sol–gel immobilization, using binary or ternary mixtures of various organosilane precursors clearly showed that sol–gel matrices formed from appropriate precursor mixtures can substantially enhance the catalytic potential of the enzymes.[19,20]

An additional strategy for boosting enzyme activity during the entrapment procedure itself was the modification of the shape of the active site by molecular imprinting using the substrates or their analogues.[21–24] In the case of CaLB, two aspects of this strategy were revealed: (i) stabilization of the active conformation of the enzyme; and (ii) supply of extra room, left after the removal of the good imprinting molecules, for the mobile lids covering the active site.[25,26]

The well-known methodology of experimental design – based on the statistical analysis of outcomes – permits the minimization of experimental efforts needed to optimize such a complex system. With the aid of response surface graphics based on a mixture model, the optimal component combination can be explored.[27] There are several reports on the application of the mixture experimental design related to biotransformations,[28,29] but the mixture experimental design for sol–gel immobilization of enzymes is an unexplored field.

In this paper, our aim was to introduce a novel approach in the development of sol–gel immobilized forms of enzymes. This approach which may be called "*immobilization engineering*" represents a novel way of thinking to create efficient biocatalysts. In this study, it involves two steps: (i) bioinformatics-based selection of the precursors acting also as bioimprinting agents (BIAs) and (ii) experimental design (Fig. 1). This philosophy was now adapted to the rational design of suitable ternary silane mixtures for the entrapment of CaLB ranging from the laboratory to the pilot plant scale. The efficiency and robustness of the resulting novel, industrially applicable "green" catalysts could be beneficially applied in the kinetic resolution of several racemic alcohols and amines both in batch and continuous-flow modes.

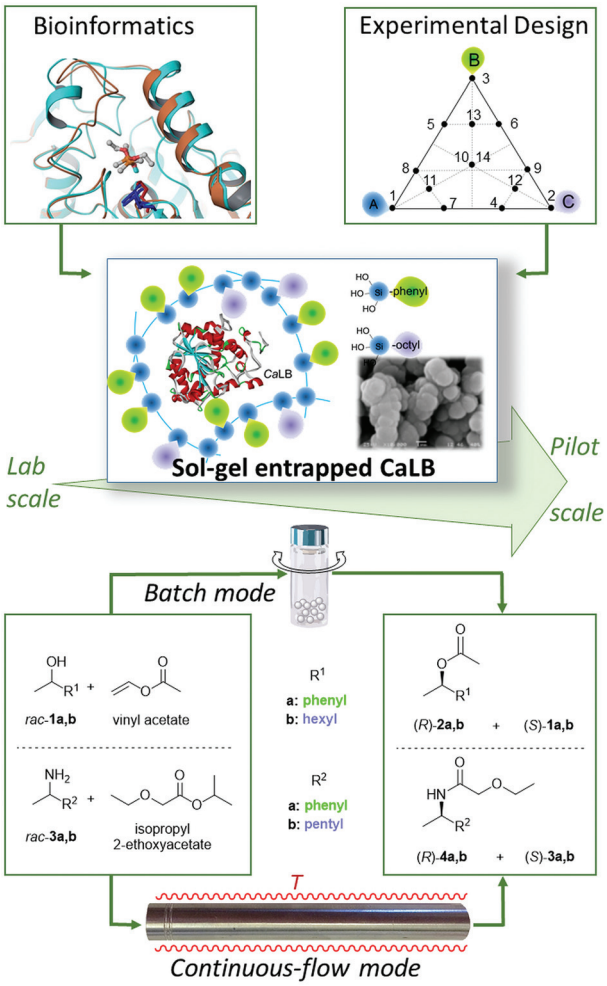

Fig. 1 Design of improved sol–gel entrapped CaLB and application of the resulting biocatalysts in kinetic resolutions of racemic alcohols and amines.

Results and discussion

Sol–gel entrapment can be regarded as a simple and robust physical immobilization method with no covalent bonding to the enzyme. The nature of organosilane precursors with different substituents (mostly alkyl and aryl groups) can significantly affect the properties of the entrapped enzyme and

the activity of the resulting biocatalysts.[19] This phenomenon is due to the combined effects of the individual organosilane precursors. On one hand, the nature of precursors can influence the morphology, permeability, and hydrophobic/hydrophilic character of the resulting sol–gel network, and on the other hand – as recent studies have shown – organosilanes can exert an imprinting effect on the enzyme altering its catalytic properties.[25,26] Thus, finding these organosilanes as components for experimental design which can exert a significant imprinting effect has become feasible by computational methods. The synergistic application of bioinformatics and experimental design tools permitted the rapid optimization of entrapment systems providing biocatalysts with improved properties (Fig. 1). By this novel "*immobilization engineering*" strategy, the development of improved sol–gel immobilized enzymes with lower environmental impact could be realized with concomitant saving of considerable time and money.

The biocatalytic properties and durability of our new preparations were evaluated in kinetic resolutions of two racemic alcohols (*rac*-**1a,b**) and two racemic amines (*rac*-**1a,b**) using acylating agents vinyl acetate and isopropyl 2-ethoxyacetate,[30] respectively, both in batch and continuous-flow systems (Fig. 1).

Selection of sol–gel precursor systems based on bioinformatics

To find organosilanes serving not only as entrapment matrix precursors but also as bioimprinting agents, binding poses of several partially hydrolyzed organosilanes were predicted within the open and closed lid structures of CaLB (PDB code: 5A6V; Table 1).[31] Our previous modeling studies, concerning the active sites of the open-lid and closed-lid conformations of CaLB, could rationalize the bioimprinting effects of various BIAs for the following two reasons:[26] the most effective BIAs are supposed (i) to conserve the reactive conformation of the active site and (ii) to provide enough space for the necessary lid movements at the active site. Thus, efficient BIAs, mimicking the substrate, exert favorable stabilizing interactions with residues in the active site.[26]

In this study, a complex method was introduced to model the effects of BIAs. This protocol was based on our previous, exploratory method,[26] by applying induced-fit docking and subsequent scoring with a modified version of the molecular mechanics-based generalized Born and surface area continuum solvation method (MM-GBSA, simply referred to as ΔE_b).

In the present study within the open-lid structure of CaLB each of the partially hydrolyzed silanes behaved similarly, in full agreement with our previous study.[26] Within the open lid structure of CaLB, docking revealed only substrate mimicking poses. Every silane precursor occupied the active site and formed hydrogen bonds with the catalytic triad and its close proximity (structures are not shown, for binding energies see $\Delta E_{b\text{-}o}$ in Table 1).

Within the closed-lid loop structure of CaLB docking revealed the already identified substrate mimicking poses.[26] In addition, several partially hydrolyzed silanes could occupy multiple poses interacting directly with the lid-loop. These results reproduced our previous finding,[26] albeit with modest differences, namely that certain silane precursors were capable not only to stabilize the active site but also to provide more room for lid-loop movements (Fig. 2 [32]).

Consequently, our screening was focused on selecting these particular precursors which can adopt both binding poses in the closed-lid form of CaLB with high affinities, but slightly preferring the lid-loop-interacting pose ($\Delta\Delta E_{b\text{-}cc\text{-}cl}$ in the range of −2–6 kcal mol^{-1}). Balanced affinity was important to manifest both effects with comparable frequency. The major enhancement in the biocatalyst's activity, however, was expected from the enlarged space for the lid-loop movements after the entrapment of enzymes complexed with BIAs in lid-loop-interacting poses. In Table 1, binding energies of the partially hydrolyzed forms of the potential silane precursors are presented within the open- and closed-lid conformations of CaLB. As shown by us earlier,[26] the binding affinity was higher for almost all of the silanes investigated within the closed-lid loop CaLB than those calculated for the open-lid variant.

On the basis of the above considerations, the four organosilanes resulting in partially hydrolyzed forms with $\Delta\Delta E_{b\text{-}cc\text{-}cl}$ in the range of −2–6 kcal mol^{-1} (tetraethoxysilane, phenyltriethoxysilane, dimethyldiethoxysilane, and octyltriethoxysilane; TEOS, PTEOS, DMDEOS, and OTEOS, respectively) were selected for further investigations.

Table 1 Binding energy values of various partially hydrolyzed silane precursors in open-lid and closed-lid conformations of CaLB (refined models of 5A6V chain A and chain B, respectively)

R[a]	$\Delta E_{b\text{-}o}$[b]/ kcal mol^{-1}	$\Delta E_{b\text{-}cc}$[c]/ kcal mol^{-1}	$\Delta E_{b\text{-}cl}$[d]/ kcal mol^{-1}	$\Delta\Delta E_{b\text{-}cc\text{-}cl}$[e]/ kcal mol^{-1}
Octadecyl	−27.1	−56.6	−16.6	−40.0
Propyl	−30.1	−30.7	−26.5	−4.2
—	−27.3	−31.2	−29.9	−1.3
Phenyl	−23.2	−29.0	−31.0	2.0
Dimethyl	−17.9	−24.7	−27.0	2.3
Octyl	−21.8	−28.1	−33.3	5.2
Decyl	−15.5	−27.8	−34.1	6.3
Vinyl	−25.3	−25.7	−33.2	7.5
Methyl	−32.0	−29.9	−42.7	12.8
Dodecyl	−23.4	[f]	−36.6	—
Hexyl	−25.6	−23.1	[f]	—

[a] Substituent(s) in partially hydrolyzed alkoxysilanes [$Si(OEt)_2(OH)_2$, R-$Si(OEt)(OH)_2$ or R_2-$Si(OEt)(OH)$]. [b] Binding energy values within an open-lid CaLB structure. [c] Binding energy values within the active centre of the closed-lid CaLB structure in the substrate mimicking pose. [d] Binding energy values within the active centre of the closed-lid CaLB structure in the lid-bound pose. [e] Differences of binding energy values of lid-bound and substrate mimicking poses in the closed-lid CaLB structure. [f] No such pose was identified by the docking calculations.

Optimization of the entrapment of CaLB in ternary sol–gel systems by experimental design

In a mixture experiment, the independent variables are the proportions of the components.[27] Because TEOS should be present as the major bulking component in all compositions, the four selected organosilane precursors define three possible ternary compositions for the sol–gel entrapment of CaLB.

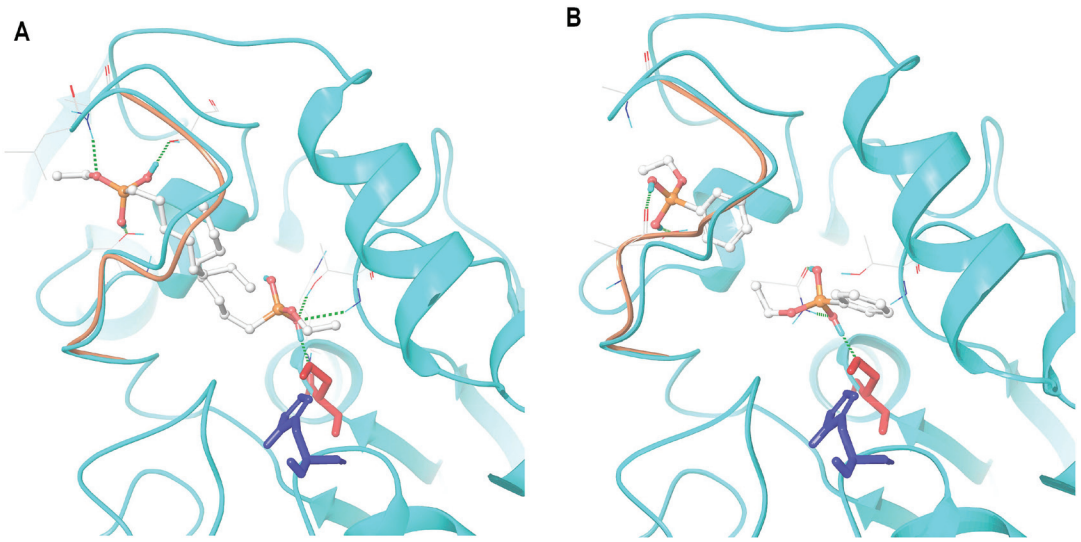

Fig. 2 Major docking poses of two partially hydrolyzed silane precursors, (A) $PhSi(OEt)(OH)_2$ (hydrolyzed form of PTEOS) and (B) $CH_3(CH_2)_7Si(OEt)(OH)_2$ (hydrolyzed form of OTEOS) in CaLB with closed lid conformation (refined model of 5A6V: chain B). In both panels, the full structure with the bound molecule mimicking the pose of a substrate is in cyan, the loop in the model with the bound molecule in lid loop-interacting pose is in light brown, Ser130 is colored in red and His249 in blue. Images were created by Maestro.[31]

Since the nature of the silane precursors, as well as their molar ratio affected the catalytic potency of the entrapped enzyme, experimental design for multi-component mixtures was applied to optimize the sol–gel systems of the selected ternary compositions.

CaLB biocatalysts entrapped in sol–gel matrices having compositions suggested by the experimental design were tested in kinetic resolutions (KR) of racemic alcohols (*rac*-**1a,b**; with vinyl acetate) and racemic amines (*rac*-**3a,b**; with isopropyl 2-ethoxyacetate) (Fig. 1 and 3). Stable matrix formation required the addition of a small amount of TEOS (min. 12 n/n%) (Fig. 3).

The productivity of the biocatalysts in batch systems as a dependent variable was characterized by the so-called specific reaction rate (r_{batch}).[33] Normal probability plots and residuals *vs.* fitted value plots for the three ternary silane precursor systems (Fig. S7–S9 in the ESI†) showed that the residuals were good approximations for the normal distribution and no specific tendencies or effects caused by external factors were found. First, CaLB entrapment in the TEOS/OTEOS/PTEOS (**TOP**) precursor system was investigated (Fig. 3 and Table S7†). Notably, in the kinetic resolution (KR) of aromatic alcohol *rac*-**1a**, the best conversions and enantiomeric excess (ee) values were achieved by CaLB entrapped in the ternary compositions of sol–gel forming precursors (Table S7:† Point 10, $c_{\mathbf{1a}}$ = 15.8%; Point 13, $c_{\mathbf{1a}}$ = 17.8% and Point 14: $c_{\mathbf{1a}}$ = 14.5% with $ee_{(R)\text{-}\mathbf{2a}}$ = 99.5% for each). With the aliphatic alcohol *rac*-**1b**, CaLB entrapped in a binary sol–gel with the highest octylsilane content was the most efficient (Table S7:† Point 2, $c_{\mathbf{1b}}$ = 34.5%, $ee_{(R)\text{-}\mathbf{2b}}$ = 99.7%) while less of octylsilane in the composition decreased conversion rates. Thus, in KRs of secondary alcohols *rac*-**1a,b**, an interesting phenomenon was observed. The predominance of a phenyl substituted precursor provided the highest activity for the entrapped CaLB in KR of a phenyl substituted substrate (*rac*-**1a**, Fig. 3A), but CaLB entrapped in a matrix with the octyl-silane predominance was more active in the KR of the alcohol with aliphatic substituents (*rac*-**1b**, Fig. 3B). In the case of *rac*-**1b**, the **TOP** system (Fig. 3B) showed a special cubic character in which in addition to TEOS/OTEOS and OTEOS/PTEOS interactions, one involving the three precursors was found. KR of amines *rac*-**3a,b** showed a shift in activity maxima towards lower hydrophobicity values of the sol–gel matrix (higher TEOS content, see Point 7 in fig. panels 3C, 3D and in Table S7,† x_{TEOS} = 0.706). Similar to the case of aliphatic alcohol *rac*-**1b**, a CaLB preparation entrapped in a sol–gel system with an aliphatic silane component (OTEOS) was optimal for high conversions in the KR of aliphatic amine *rac*-**3b**, although at higher hydrophilicity (lower proportion of OTEOS: Point 7, x_{OTEOS} = 0.294 in Fig. 3D for *rac*-**3b** compared to Point 2, x_{OTEOS} = 0.880 in Fig. 3B for *rac*-**1b**). Compositions of lower hydrophobicity in the TOP system were also the most productive for the aromatic amine *rac*-**3a** (Point 7, x_{TEOS} = 0.706, Fig. 3C).

Models for *rac*-**1b** with the systems TEOS/DMDEOS/OTEOS (**TDO**, Fig. 3J) and TEOS/DMDEOS/PTEOS (**TDP**, Fig. 3F) were quadratic too. DMDEOS also had a significant effect for both alcohols *rac*-**1a,b** in the **TDO** (Fig. 3I and J) and **TDP** (Fig. 3E and F) systems, but similar to the **TDP** system, high hydrophobicity (high proportion of OTEOS) had an important impact on biocatalytic activity for *rac*-**1b** in the **TDO** system (Fig. 3J). In general, PTEOS with an aromatic substituent positively influenced the activity of CaLB in KR of the aromatic substrate *rac*-**1a**, while the effect of addition of OTEOS was most significant in the KR of the aliphatic substrate *rac*-**1b**.

As discussed for the KRs of amines *rac*-**3a,b** with the **TOP** system (Fig. 3C and D), a more hydrophilic composition

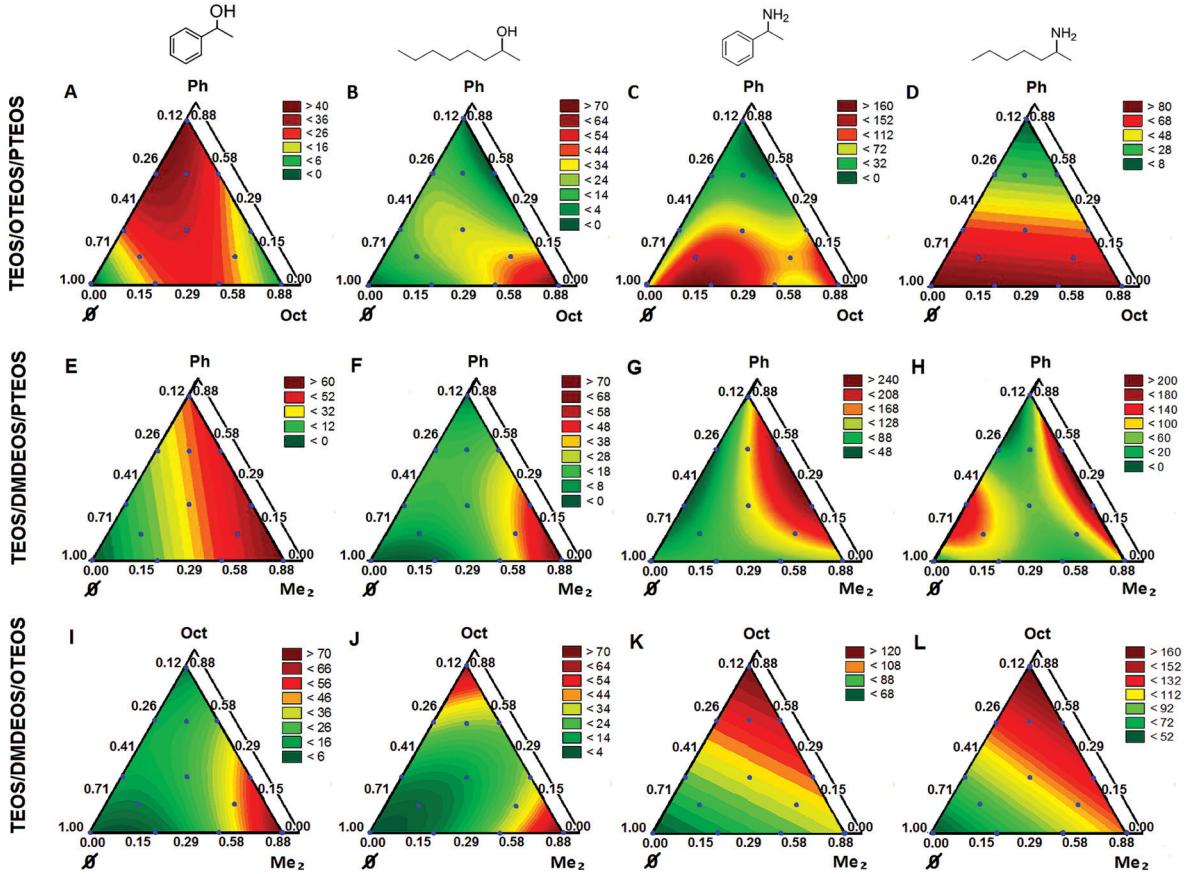

Fig. 3 Specific reaction rates (r_{batch}) with CaLB biocatalysts corresponding to the experimental design points of TEOS/OTEOS/PTEOS (**TOP**), TEOS/DMDEOS/PTEOS (**TDP**), and TEOS/DMDEOS/OTEOS (**TDO**) ternary sol–gel systems in kinetic resolutions of (A, E, I) *rac*-**1a**, (B, F, J) *rac*-**1b**, (C, G, K) *rac*-**3a** and (D, H, L) *rac*-**3b**.

favored the conversion of the more polar amines with a larger acylating agent. This effect was not simply apparent in the case of fully cubic models such as for the amine with an aromatic substituent (*rac*-**3a**) in **TOP** (Fig. 3C) and **TDO** (Fig. 3K) systems (for the significant effects, see Tables S5A and S5C,† respectively; in the ESI†). For the KR of aromatic amine *rac*-**3a** with CaLB in the **TDP** system using the three least hydrophobic precursors, the model was quadratic (Fig. 3G; for component interactions, see Table S5B, in the ESI†).

With the amine having aliphatic substituents (*rac*-**3b**), the model was linear for the **TDO** system (Fig. 3L), where only OTEOS had a strong hydrophobic character and hence the most pronounced impact on biocatalytic activity (Table S6C, in the ESI†). On the other hand, for the **TDP** system, the model was fully cubic again (Fig. 3H; for significant interactions, see Table S6B, in the ESI†).

Stability of sol–gel entrapped CaLB in batch mode

Mechanical, thermal and chemical (operational) stabilities are of prime importance in biocatalysis. In stirred tank reactors – typical of batch reactions – the catalyst is under significant mechanical stress causing serious deactivation. This effect is mostly avoided using continuous-flow packed-bed reactors.[33]

Immobilization yield is an important factor bearing on the economic viability of the process.[13,14] In a properly selected sol–gel entrapment matrix, the enzyme molecules remain fully fixed while the diffusion of the substrate and product molecules is barely hindered.[17,19] Sodium dodecyl sulfate polyacrylamide gel electrophoresis (SDS-PAGE) analysis of our sol–gel-entrapped biocatalyst indicated no leakage of CaLB after immobilization (Fig. S10 in the ESI†).

The reusability of selected CaLB biocatalysts entrapped in three different sol–gel systems using different ternary compositions of organosilanes (Point 10 of the models **TOP**, **TDP**, and **TDO**, see Table S2† and Fig. 3) were compared with the commercially available immobilized versions of CaLB [Immobead-T2-150: covalently attached to polyacrylic resin (CV-T2-150) and Novozyme 435: CaLB adsorbed onto macroporous polyacrylic resin (N 435)] in multi-cycle KRs of *rac*-**1a** (section 3.2. in the ESI†). All three versions of the sol–gel entrapped CaLB preparations were more durable in recycling tests than the commercial formulations (Fig. 4). Particularly, **TOP**-10 CaLB proved to be quite durable in the recycling tests, retaining after 10 cycles more than 91% of its initial activity (Fig. 4). The polyacrylic bead-based CaLB biocatalysts CV-T2-150 and N 435 (particle size of 150–500 μm) were less stable, mainly due to disintegrating to less

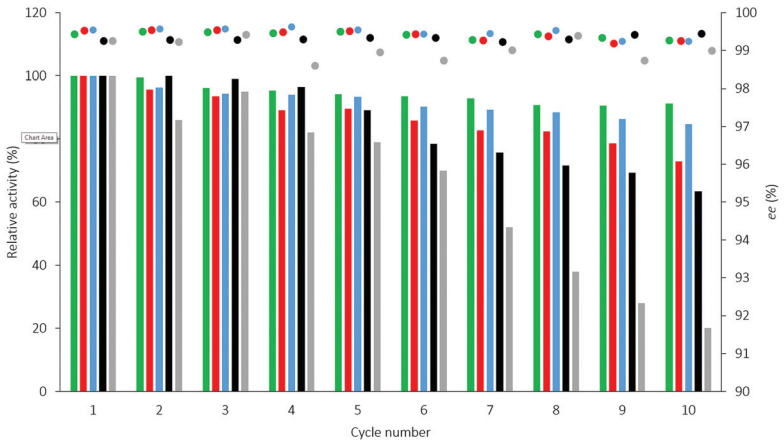

Fig. 4 Reusability of the immobilized CaLB biocatalysts in KR of *rac*-**1a** [immobilized CaLB forms in 1 h cycles: **TOP**-10 (U_B: ■, ee% ●), **TDP**-10 (U_B: ■, ee% ●), **TDO**-10 (U_B: ■, ee% ●), N 435 (U_B: ■, ee% ●), CV-T2-150 (U_B: ■, ee% ●)].

active smaller fragments (Fig. 4: residual activities were 20% for CV-T2-150 and 64% for N 435 after 10 cycles).[34] Mie scattering of the sol–gel entrapped CaLBs after ultrasonication – compared to their initial states – proved that these CaLB biocatalysts comprised quite stable particles (with 10–100 μm particle size range, see section 7 and Fig. S13, in the ESI†).

Heat tolerance and operational stability of the biocatalyst are important features which can be much enhanced by immobilization. Heat tolerance of three selected CaLB biocatalysts (Point 10 of the models **TOP**, **TDP**, and **TDO**) and two commercially available immobilized CaLB forms, CV-T2-150 and N 435, were compared by KR of *rac*-**1a** over a wide range of temperatures (30–100 °C, Fig. 8). While up to 50 °C, all of them were thermostable, above this temperature the activity of the various CaLB forms decreased differently. **TDO**-10 CaLB retained its high activity up to 100 °C (limited to r_{batch} = 94.4 U g^{-1} due to reaching 50% conversion in the KR of *rac*-**1a**) (Fig. 5A) with excellent enantiomer selectivity (Fig. 5B, $ee_{(R)\text{-}2a}$ > 99%). Even the least durable of the new biocatalyst *i.e.* **TOP**-10 CaLB worked at acceptable activity at 100 °C (Fig. 5A, r_{batch} = 40.9 U g^{-1}) *i.e.* at >60% of the initial specific reaction rate (Fig. 8a) and $ee_{(R)\text{-}2a}$ >98% (Fig. 5B). At >80 °C, the performance of CaLB in both OTEOS-containing systems (**TOP**-10 and **TDO**-10 CaLB) was superior to that of the commercial CaLB forms regarding both activity and enantiomer selectivity (Fig. 5).

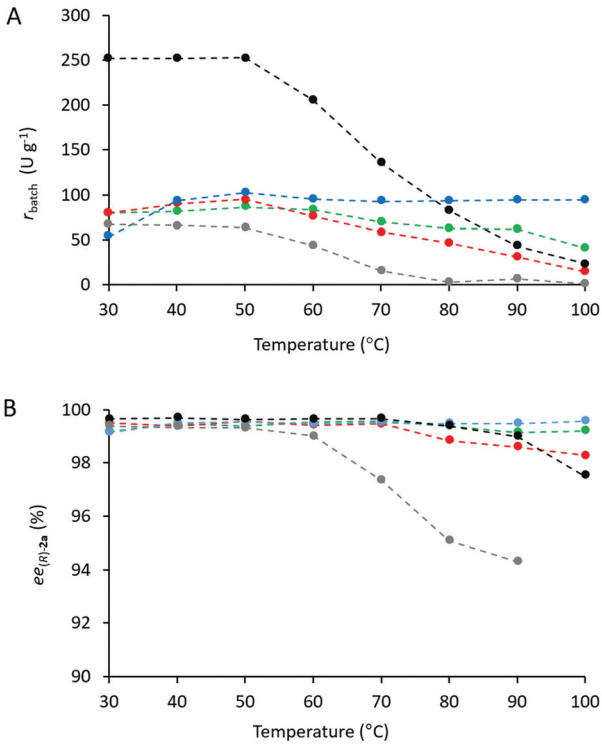

Fig. 5 Changes of (A) specific reaction rate (r_{batch}) and (B) enantiomeric excess of the product [$ee_{(R)\text{-}2a}$] during the thermal stability test of CaLB biocatalysts [**TOP**-10 (●), **TDP**-10 (●), **TDO**-10 (●), CV-T2-150 (●), N 435 (●)] after 0.5 h reaction time in toluene.

Scale up of the sol–gel immobilization process of *Ca*LB

For industrial applications of biocatalysis, scale up of the immobilization procedure is a crucial issue where multiple technological and quality requirements must be satisfied. The conservation of catalytic activity, enantiomer selectivity and physical-chemical properties is critical.

In our study, the entrapment of CaLB in the **TDP** matrix (**TDP**-10 CaLB) was scaled up 100-fold from the usual laboratory scale (~250 mg). As the main parameters for comparison, the biocatalytic activity (U_B), enantiomeric excess of the product ($ee_{(R)\text{-}3a}$), and average particle size (D_p) of the packing were chosen (Table 2).

In addition to the usual techniques, the particle size distribution and the congruency factor of the Raman-maps (R) for the lab scale and scaled up **TDP**-10 CaLB were also investigated.

Raman spectroscopy, a non-invasive technique, is specific to the chemical bonds and symmetry of molecules.[35] Only few

Table 2 Comparison of CaLB entrapment in the **TDP**-10 sol–gel matrix on a laboratory scale (250 mg) and on 100-fold scale up

Scale	U_B/U g^{-1}	ee$_{(R)\text{-}\mathbf{3a}}$/%	D_p/μm
Lab scale	69.5	99.6	51.2
100-fold scale up	66.2	99.6	42.5

examples exist about the examination of enzymes attached to electrodes by surface-enhanced resonance Raman spectroscopy.[36] Sol–gel processes have also been characterized by Raman spectroscopy, but enzymes entrapped in sol–gel matrices have not been investigated. Raman-maps of the two preparations (section 8 and Fig. S12 in the ESI†) were compared by Pearson correlation analysis.[37] The 0.9902 value of the Pearson correlation coefficient indicated high similarity of the two systems.

The particle size analysis of the lab scale and scaled up **TDP**-10 CaLB was also investigated by Mie scattering (section 9 in the ESI†). The particle size distribution of the scaled up **TDP**-10 CaLB was similar to that found for the lab scale **TDP**-10 CaLB (Fig. S14 in the ESI†).

FT-IR analysis of the fingerprint region (450–1500 cm^{-1}) confirmed the presence of the alkyl or aryl functional groups of the precursors in the xerogels (section 11, Fig. S21–23 in the ESI†). However, similar to previous reports, FT-IR was not able to locate the enzyme.[18]

Similar to our recent work on the sol–gel entrapment of a methanol tolerant thermophilic lipase,[7] the specific surface area of the biocatalysts by N_2 adsorption/desorption did not correlate with the activity of biocatalysts (section 10, Table S11 in the ESI†).[18] N_2 adsorption could provide the surface available for small and relatively nonpolar N_2 molecules but not for larger molecules with higher polarity. Based on the SEM data however, the activity could be associated with the average length of the nanochannels, which was much shorter for a microstructured material than for a non-microstructured matrix.[18] Scanning electron microscopy (Fig. 6 and Fig. S15–S18 in the ESI†) clearly indicated that **TDP**-10 CaLB formed as ~60 μm particles (Fig. S18F and 19F†, respectively) with a porous microstructured morphology due to sticking submicron particles together (Fig. 6C and Fig. S17F in the ESI†). Therefore, the length of nanochannels with diffusion limitations within **TDP**-10 CaLB (Fig. 6C) was significantly shorter than within the other, less porous matrices such as within the TEOS matrix (Fig. 6A) or the TEOS-PTEOS binary matrix (Fig. 6B).

According to the density measurements (Table S11 in the ESI†), the TEOS-based biocatalyst (*e.g.* **TDP**-1 CaLB) had the highest density, while the densities of the binary (**TDP**-5 CaLB) and ternary systems (**TDP**-10 CaLB) were lower. In contrast, the CaLB entrapped in the TEOS-based matrix had higher total volume of pores (0.22 cm^3 g^{-1}) than CaLB entrapped in binary and ternary systems (0.05–0.09 cm^3 g^{-1}, Table S11 in the ESI†). This deviation stemmed from the limitation of the BET method which could measure pores only up to 50 nm.

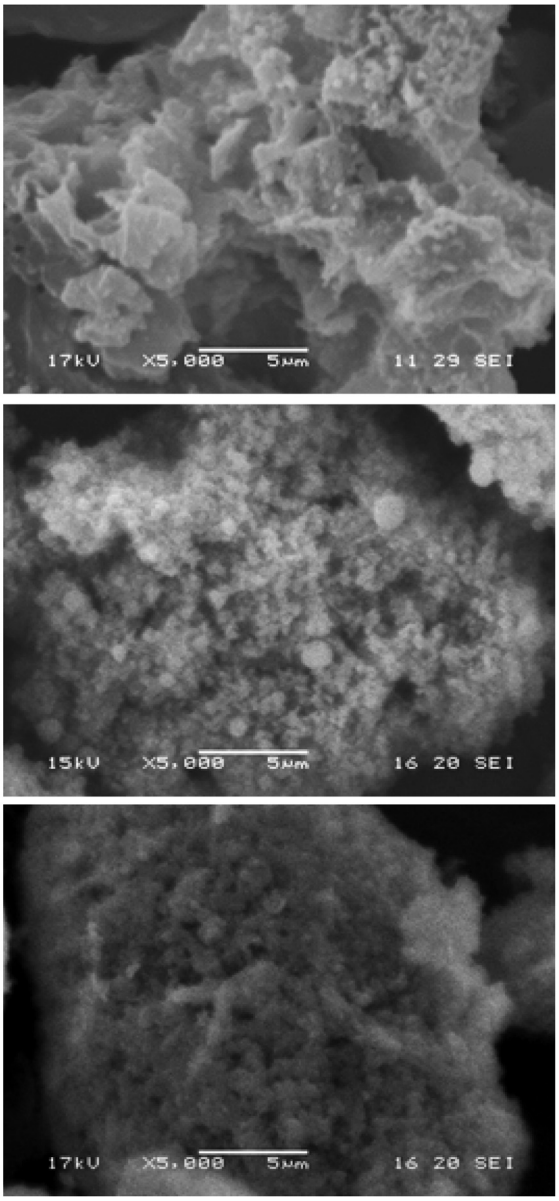

Fig. 6 SEM images of sol–gel CaLB biocatalysts entrapped within different precursor systems: TEOS matrix, **TDP**-1 (A), TEOS-PTEOS binary matrix, **TDP**-5 (B) and TEOS-DMDEOS-PTEOS ternary matrix, **TDP**-10 (C).

However, according to the density data and the SEM images, larger pores were dominant within several binary and ternary preparations.

Application of sol–gel entrapped CaLB in continuous-flow reactor systems

Continuous-flow systems are widely applied to produce fine chemicals prompted by their obvious benefits among them easy control of reaction parameters, high productivity and good reproducibility.[38] To explore the potential of the sol–gel entrapped CaLB biocatalysts in continuous-flow systems, we studied the catalytic performance of our best preparations in a

laboratory reactor system. The reactor equipped with stainless steel columns (CatCart™) packed with the most effective CaLB biocatalysts enabled the precise temperature and flow rate control. This continuously operated bioreactor system with **TOP**-10, **TDP**-10, and **TDO**-10 CaLB columns was used for kinetic resolution of racemic alcohols *rac*-**1a,b** with vinyl acetate as the acylating agent, while **TOP**-11, **TDP**-11, and **TDO**-11 CaLB columns were used in KR of amines (*rac*-**3a,b**) using isopropyl 2-ethoxyacetate as the acylating agent.[30]

In order to be able to study temperature effects in a continuous-flow system, the first series of experiments was directed to find the range of substrate concentrations where the effect could be well observed, *i.e.* conversions remaining in the linear kinetic range of 10–20% (see section 7.1 in the ESI†). Therefore, the solutions of *rac*-**1a** in toluene in the range of concentrations of 1–64 mg mL^{-1} were pumped through columns filled with **TOP**-10 CaLB, **TDP**-10 CaLB, and **TDO**-10 CaLB (Fig. 7A). On the basis of the results, 48 mg mL^{-1} concentration of *rac*-**1a** was selected to test thermal stability (Fig. 7A; for further details, see section 7.2 and Fig. S11 in the ESI†).

Temperature dependent behavior of CaLB biocatalysts (**TOP**-10, **TDP**-10, and **TDO**-10) was compared with those of commercial immobilized CaLB preparations CV-T2-150 and N 435 (Fig. 7). Thus, the solution of *rac*-**1a** (48 mg mL^{-1}) and vinyl acetate (2.76 equiv.) in toluene was pumped through the three packed-bed columns filled with the mentioned biocatalysts while raising the temperature from 30 to 100 °C in increments of 10 °C at a constant flow rate of 0.20 mL min^{-1}. The productivity (r_{flow}) (Fig. 7A) and enantiomeric excess ($ee_{(R)\text{-}2a}$) values of the product (Fig. 7B) were plotted as a function of temperature. For all of the CaLB preparations, r_{flow} – temperature curves were of quite similar shape over the entire temperature range (30–100 °C). Between 30 and 60 °C, the specific reaction rate (r_{flow}) increased significantly peaking between 50 and 70 °C followed by a drop of 25–30% of apparent activity up to 100 °C (Fig. 7A). At 60 °C, two ternary sol–gel CaLB biocatalysts, **TOP**-10 and **TDP**-10, further N 435 were the most active surpassing the sol–gel type **TDO**-10 and the covalently attached form CV-T2-150.

The other crucial feature of enzyme catalyzed reactions is their stereoselectivity, permitting the production of chiral molecules in an enantiopure form. As it is shown in Fig. 7B, for all the five immobilized CaLB biocatalysts the enantiomeric excess ($ee_{(R)\text{-}2a}$) of the product (*R*)-**2a** decreased with increasing temperature over the entire temperature range covered. In fact, remarkably high $ee_{(R)\text{-}2a}$ values could be attained with the three ternary sol–gel CaLB biocatalysts (**TOP**-10, **TDP**-10 and **TDO**-10) which remained up to 100 °C quite high (>99%), while $ee_{(R)\text{-}2a}$ with the commercial CaLB preparations dropped below 99% at 100 °C.

Finally, the long term operational stability of **TDP**-10 CaLB was tested in the kinetic resolution of the alcohol *rac*-**1a** and the amine *rac*-**3a** in a continuous-flow reactor at 60 °C using toluene as a solvent (Fig. 8). The operation of both KRs remained stable over 5 day-long continuous runs at this temperature, indicating the robustness of **TDP**-10 CaLB in continuous-flow mode biotransformations. After proper separation, the products were isolated in good yields (47%, for both) and high enantiomeric purity (ee 99.7%, and 99.9%), for (*R*)-**2a** and (*R*)-**4a**, respectively; (for details of analysis on a small analytical scale, see section 6.2 and Table S10 in the ESI†).

Space time yield[39] and specific enzyme productivity analysis revealed the applicability of the CaLB preparations entrapped

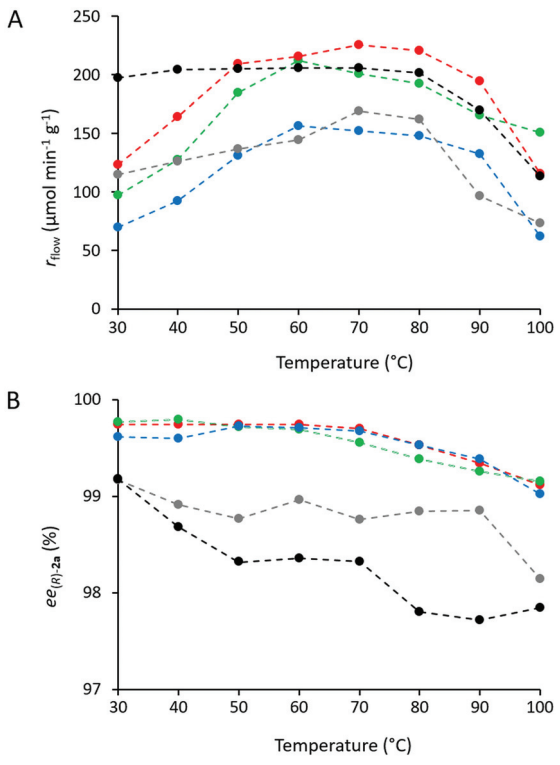

Fig. 7 Temperature dependence of (A) specific reaction rate (r_{flow}) and (B) enantiomeric excess of the product ($ee_{(R)\text{-}2a}$) in continuous-flow kinetic resolution of *rac*-**1a** (48 mg mL^{-1}) catalyzed by differently immobilized CaLBs [TOP-10 (●), TDP-10 (●), TDO-10 (●), CV-T2-150: (●), N 435: (●)] in dry toluene.

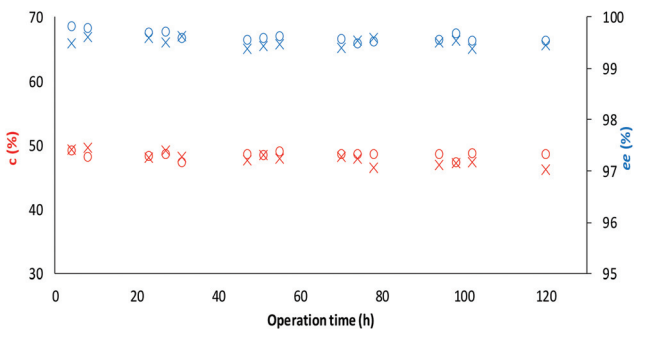

Fig. 8 Long term stability of the CaLB entrapped in the TDP sol–gel system in KR of the alcohol *rac*-**1a** (c%: x, $ee_{(R)\text{-}2a}$: x) and amine *rac*-**3a** (c%: ○, $ee_{(R)\text{-}4a}$: ○) in a continuous-flow reactor (60 °C, flow-rate of 0.1 mL min^{-1}).

Table 3 Space-time yield and specific productivity of CaLB entrapped in various sol–gel matrices for kinetic resolutions of the selected alcohol and amine substrates (*rac*-**1a,b** and *rac*-**3a,b**) in continuous-flow mode

Substrate	Biocatalyst	Y_s[a]/kg L^{-1} h^{-1}	U_E[b]/kg g^{-1} day^{-1}
rac-**1a**	**TDP**-10 CaLB	0.81	0.44
rac-**1b**	**TOP**-10 CaLB	1.08	0.53
rac-**3a**	**TOP**-10 CaLB	1.01	0.51
rac-**3b**	**TDO**-10 CaLB	1.21	0.66

[a] Space time yield (Y_s). [b] Specific productivity of the enzyme (U_E).

in rationally engineered ternary sol–gel matrices as green biocatalysts (Table 3). Thus, assuming *e.g.* that the durability of the **TDP**-10 CaLB is independent of the flow rate, 1 g of native CaLB is applicable in its sol–gel entrapped form in 5 days to produce 2.2 kg of (*R*)-**2a** with an ee of 99.4% (from a KR with a conversion of 28.5%, at a flow rate of 0.6 ml min^{-1}) or 3.3 kg of (*R*)-**4a** with an ee of 99.8% (from a KR with a conversion of 28%, at a flow rate of 0.6 ml min^{-1}).

Experimental

Materials and methods

Details on materials, enzymes and analytical methods used in this study are provided in the ESI.†

Sol–gel immobilization of CaLB using binary or ternary silane precursor systems. Aqueous PEG 1000 solution (4 m/m%, 200 μL) and 2-propanol (200 μL) were added to sodium phosphate buffer (0.1 M, pH 7.5, 390 μL) in a 20 ml glass vial and the mixture was shaken at 450 rpm. After 5 min of shaking at room temperature, a composition of the silane precursors (for compositions see Table S2 in the ESI†), lyophilized CaLB (50 mg) and 1 M aqueous sodium fluoride solution (100 μL) were added to the mixture and shaking was maintained for 24 h at room temperature. Then the samples were washed – by suspending (1 min) and filtration on a glass filter (G4) – with isopropanol (7 mL), distilled water (5 mL), isopropanol (5 mL) and *n*-hexane (5 mL). The white powdery product was air-dried at room temperature for 24 h and stored in a refrigerator (4 °C).

Evaluation of the catalytic properties of the sol–gel entrapped CaLB biocatalysts in kinetic resolution of alcohols *rac*-1a,b. Native or sol–gel immobilized CaLB (25 mg) was added to the solution of the racemic alcohol (*rac*-**1a** or *rac*-**1b** 50 μL) and vinyl acetate (100 μL) in *n*-hexane : methyl *t*-butyl ether 2 : 1 (v/v, 1 mL), and the mixture was shaken at 30 °C in a sealed glass vial at 750 rpm.

For GC analyses of the enantiomeric composition of **1a,b** and **2a,b**, after 0.5 h and 1 h samples (20 μL) were taken directly from the reaction mixture, diluted with ethanol (980 μL) and analyzed on an Agilent 4890 GC equipped with a Hydrodex β-6TBDM column and flame ionization detector. For detailed results see sections 1.6 in the ESI.†

Evaluation of the catalytic properties of the sol–gel entrapped CaLB biocatalysts in kinetic resolution of amines *rac*-3a,b. Native or sol–gel immobilized CaLB (20 mg) was added to the solution of the racemic amine (*rac*-**3a** or *rac*-**3b**, 100 μL) and isopropyl 2-ethoxyacetate[30] (60 μL) in dry toluene (2 mL), and the mixture was shaken at 30 °C in a sealed glass vial at 750 rpm.

For GC analyses of the enantiomeric composition of **3a,b** and **4a,b** after 0.5 and 1 h samples (20 μL) were taken directly from the reaction mixture, diluted with ethanol (980 μL) and analyzed on an Agilent 4890 GC equipped with a Hydrodex β-6TBDM column and a flame ionization detector and on an Agilent 5890 GC equipped with a Hydrodex β-TBDAc column and a flame ionization detector. For detailed data see section 1.6 in the ESI.†

Kinetic resolution of alcohols *rac*-1a,b and amines *rac*-3a,b in continuous-flow mode. Experiments were performed in a laboratory scale flow reactor comprising within an in-house made multicolumn thermostated aluminum metal block holder with precise temperature control (Lauda, Alpha RA8) three packed-bed CatCart™ columns filled with the immobilized CaLB biocatalysts and attached to HPLC pumps. Before use, the columns were washed with toluene (0.5 mL min^{-1}, 30 min). For further details, see section 7 in the ESI.†

Conclusions

Our study using "immobilization engineering" focused on the rational improvements of the sol–gel enzyme entrapment process with the aid of bioinformatics and experimental design tools.

Molecular docking and modeling was applied as a part of the immobilization engineering method. Modeling within the open-lid and closed-lid conformations of lipase B from *Candida antarctica* enabled efficient selection of organosilanes serving as components of ternary compositions to prepare sol–gel matrices for the entrapment of CaLB, an enzyme widely applied in various industrial processes.

Immobilization engineering was further aided by the *response surface methodology* leading to novel ways of CaLB immobilization with enhanced functional efficiency and reusability.

The novel biocatalysts were prepared by entrapment of CaLB in sol–gel matrices using three different ternary compositions of organosilanes. The systems were tested in kinetic resolution of two racemic alcohols and two racemic amines. The rational selection of the organosilane precursors enabled the preparation of highly efficient and enantioselective biocatalysts. We also found that there exists no single "*best*" silane precursor composition and each substrate requires individual optimization. Therefore, our approach, a combination of computational and experimental methods which can highly accelerate the optimization process, is of general importance and can significantly contribute to the dissemination of an inherently green methodology.

In the kinetic resolution of secondary alcohols and secondary amines substituted with aromatic or aliphatic substituents, sol–gel-entrapped CaLBs were superior to the traditional polymer-based forms. They are characterized by enhanced thermal stability in organic media, improved recyclability and higher operational stability both in batch and continuous mode operations.

The space–time yield in the range of 0.81–1.21 kg L^{-1} h^{-1} and the specific productivity in the range of 0.44–0.66 kg g^{-1} day^{-1} observed with the various sol–gel entrapped forms of CaLB in continuous-mode KRs of selected alcohol and amine substrates as well as facile scaling up of the immobilization process (up to 100-fold from the lab scale) and the potential to produce more than 2.5 kg product per g native enzyme make our method a tunable and economical green option to produce biocatalysts for flow chemistry.

Acknowledgements

The financial support from the New Hungary Development Plan (TÁMOP-4.2.1/B-09/1/KMR-2010-0002) is acknowledged. Licensing of the Schrödinger Suite software package was financed by the Hungarian OTKA Foundation (K 108793). WD thanks the UNKP-PD-416 program for the financial support. We thank Prof. Mihály Nógrádi (BME, Budapest) for helpful discussions.

References

1 *Biocatalysis for green chemistry and chemical process development*, ed. J. A. Tao and R. Kazlauskas, John Wiley & Sons, Inc., Hoboken, 2011.

2 (*a*) L. Poppe and L. Novák, *Selective Biocatalysis: A Synthetic Approach*, Verlag Chemie, Weinheim-New York, 1992; (*b*) J. Whittall and P. Suton, *Practical methods for biocatalysis and biotransformations*, Wiley, Chichester, 2010.K. Faber, *Biotransformations in Organic Chemistry*, Springer, New York, 6th edn, 2011.

3 H. P. Meyer, O. Ghisalba and J. E. Leresche, in *Green Catalysis – Biocatalysis (Volume 3)*, ed. R. H. Crabtree, Wiley-VCH Verlag GmbH & Co. KGaA, Weinheim, 2009, pp. 171–212.

4 (*a*) U. T. Bornscheuer, G. W. Huisman, R. J. Kazlauskas, S. Lutz, J. C. Moore and K. Robins, *Nature*, 2012, **485**, 185–194; (*b*) A. Currin, N. Swainston, P. J. Day and D. B. Kell, *Chem. Soc. Rev.*, 2015, **44**, 1172–1239.

5 (*a*) M. T. Reetz, *Curr. Opin. Chem. Biol.*, 2002, **6**, 145–150; (*b*) U. T. Bornschauer and R. J. Kazlauskas, *Catalytic promiscuity in biocatalysis: using old enzymes to form new bonds and follow new pathways*, Wiley-VCH, Weinheim, New York, 2004; (*c*) U. T. Bornscheuer and R. J. Kazlauskas, *Hydrolases in organic synthesis: regio- and stereoselective biotransformations*, Wiley-VCH, New York-Weinheim, 2nd edn, 2006.

6 T. Tan, J. Lu, K. Nie, L. Deng and F. Wang, *Biotechnol. Adv.*, 2010, **28**, 628–634.

7 S. Gihaz, D. Weiser, A. Dror, P. Sátorhelyi, M. Jerabek-Willemsen, L. Poppe and A. Fishman, *ChemSusChem*, 2016, **9**, 3161–3170.

8 K. P. Dhake, D. D. Thakare and B. M. Bhanage, *Flavour Fragrance J.*, 2013, **28**, 71–83.

9 Z. S. Olempska-Beer, R. I. Merker, M. D. Ditto and M. J. DiNovi, *Regul. Toxicol. Pharmacol.*, 2006, **45**, 144–158.

10 E. E. Jacobsen and T. Anthonsen, *Int. J. Chem.*, 2012, **4**, 7–13.

11 E. M. Anderson, K. M. Larsson and O. Kirk, *Biocatal. Biotransform.*, 1997, **16**, 181–204.

12 V. G. Fernández, E. Busto and V. Gotor, *Adv. Synth. Catal.*, 2006, **348**, 797–812.

13 R. A. Sheldon, *Chem. Soc. Rev.*, 2012, **41**, 1437–1451.

14 (*a*) *Immobilization of enzymes and cells*, ed. J. M. Guisan, Humana Press Inc., Totowa, NJ, 2nd edn, 2006; (*b*) R. A. Sheldon, *Adv. Synth. Catal.*, 2007, **349**, 1289–1307; (*c*) H. Noureddini and X. Gao, *J. Sol-Gel Sci. Technol.*, 2007, **41**, 31–41; (*d*) U. Hanefeld, L. Gardossi and E. Magner, *Chem. Soc. Rev.*, 2009, **38**, 453–468; (*e*) C. Garcia-Galan, A. Berenguer-Murcia, R. Fernandez-Lafuente and R. C. Rodrigues, *Adv. Synth. Catal.*, 2011, **353**, 2885–2904; (*f*) D. N. Tran and K. J. Balkus Jr., *ACS Catal.*, 2011, **1**, 956–968; (*g*) S. Datta, L. R. Christana and Y. R. S. Rajaram, *3 Biotech.*, 2013, **3**, 1–9; (*h*) R. A. Sheldon and S. van Pelt, *Chem. Soc. Rev.*, 2013, **42**, 6223–6235; (*i*) A. Liese and L. Hilterhaus, *Chem. Soc. Rev.*, 2013, **42**, 6236–6349; (*j*) N. R. Mohamada, N. H. Che Marzukia, N. A. Buanga, F. Huyopb and R. A. Wahab, *Biotechnol. Biotechnol. Equip.*, 2015, **29**, 205–220.

15 A. Pal and F. Khanum, *Proc. Biochem.*, 2011, **46**, 1315–1322.

16 (*a*) L. L. Hench and J. K. West, *Chem. Rev.*, 1990, **90**, 33–72; (*b*) I. Gill and A. Ballesteros, *J. Am. Chem. Soc.*, 1998, **120**, 8587–8598; (*c*) D. Avnir, T. Coradin, O. Lev and J. Livage, *J. Mater. Chem.*, 2006, **16**, 1013–1030; (*d*) S. Braun, S. Rappoport, R. Zusman, D. Avnir and M. Ottolenghi, *Mater. Lett.*, 2007, **61**, 2843–2846.

17 (*a*) D. Avnir, S. Braun, O. Lev and M. Ottolenghi, *Chem. Mater.*, 1994, **6**, 1605–1614; (*b*) A. C. Pierre, *Biocatal. Biotransform.*, 2004, **22**, 145–170; (*c*) P. Tielmann, H. Kierkels, A. Zonta, A. Ilie and M. T. Reetz, *Nanoscale*, 2014, **6**, 6220–6228.

18 C. Paul, P. Borza, A. Marcu, G. Rusu, M. Bîrdeanu, S. M. Zarcula and F. Péter, *Nanomater. Nanotechnol.*, 2016, **6**, 3.

19 (*a*) M. T. Reetz, A. Zonta, V. Vijayakrishnan and K. Schimossek, *J. Mol. Catal. A: Chem.*, 1998, **134**, 251–258; (*b*) M. T. Reetz, A. Zonta and J. Simpelkamp, *Biotechnol. Bioeng.*, 1996, **49**, 527–534; (*c*) A. Tomin, D. Weiser, G. Hellner, Z. Bata, L. Corici, F. Péter, B. Koczka and L. Poppe, *Proc. Biochem.*, 2011, **46**, 52–58; (*d*) D. Weiser, Z. Boros, G. Hornyánszky, A. Tóth and L. Poppe, *Proc. Biochem.*, 2012, **47**, 428–434.

20 A. Ursoiu, C. Paul, T. Kurtán and F. Péter, *Molecules*, 2012, **17**, 13045–13061.

21 F. H. Dickey, *Proc. Natl. Acad. Sci. U. S. A.*, 1949, **35**, 227–229.
22 J. O. Rich, V. Mozhaev, J. S. Dordick, D. S. Clark and Y. L. Khmelnitsky, *J. Am. Chem. Soc.*, 2002, **124**, 5254–5255.
23 I. Mingarro, C. Abad and L. Braco, *Proc. Natl. Acad. Sci. U. S. A.*, 1995, **92**, 3308–3312.
24 X. Cao, J. Yang, L. Shu, B. Yu and Y. Yan, *Proc. Biochem.*, 2009, **44**, 177–182.
25 G. Hellner, Z. Boros, A. Tomin and L. Poppe, *Adv. Synth. Catal.*, 2011, **353**, 2481–2491.
26 D. Weiser, P. L. Sóti, G. Bánóczi, V. Bódai, B. Kiss, Á. Gellért, Z. K. Nagy, B. Koczka, A. Szilágyi, G. Marosi and L. Poppe, *Tetrahedron*, 2016, **72**, 7335–7342.
27 (*a*) J. A. Cornell, *Experiments with Mixtures: Designs, Models, and the Analysis of Mixture Data*, John Wiley & Sons, Inc., New York, 3rd edn, 2002; (*b*) R. Lazic, *Design of Experiments in Chemical Engineering*, Wiley-VCH Verlag GmbH & Co. KGaA, Weinheim, 2004; (*c*) A. Pal and F. Khanum, *Process Biochem.*, 2011, **46**, 1315–1322; (*d*) D. Kishore and A. M. Kayastha, *Food Chem.*, 2012, **134**, 1650–1657.
28 S. Suwannarangsee, B. Bunterngsook, J. Arnthong, A. Paemanee, A. Thamchaipenet, L. Eurwilaichitr, N. Laosiripojana and V. Champreda, *Bioresour. Technol.*, 2012, **119**, 252–261.
29 F. F. G. Dias, R. J. S. de Castro, A. Ohara, T. G. Nishide, M. P. Bagagli and H. H. Sato, *Biocatal. Agric. Biotechnol.*, 2015, **4**, 528–534.
30 M. Oláh, Z. Boros, G. Hornyánszky and L. Poppe, *Tetrahedron*, 2016, **72**, 7249–7255.
31 B. Stauch, S. J. Fisher and M. J. Cianci, *J. Lipid Res.*, 2015, **56**, 2348–2358.
32 Maestro, Schrödinger, LLC, New York, NY, USA, 2015.
33 C. Csajági, G. Szatzker, E. R. Tőke, L. Ürge, F. Darvas and L. Poppe, *Tetrahedron: Asymmetry*, 2008, **19**, 237–246.
34 P. Sóti, D. Weiser, T. Vígh, Z. K. Nagy, L. Poppe and G. Marosi, *Bioprocess Biosyst. Eng.*, 2016, **39**, 449–459.
35 A. Rygula, K. Majzner, K. M. Marzec, A. Kaczor, M. Pilarczyk and M. Baranksa, *J. Raman Spectrosc.*, 2013, **44**, 1061–1076.
36 M. Sezer, P. Kielb, U. Kuhlmann, H. Mohrmann, C. Schulz, D. Heinrich, R. Schlesinger, J. Heberle and I. M. Weidinger, *J. Phys. Chem. B*, 2015, **119**, 9586–9591.
37 K. Pearson, *Proc. R. Soc. London*, 1895, **58**, 240–242.
38 (*a*) G. Jas and A. Kirschning, *Chem. – Eur. J.*, 2003, **9**, 5708–5723; (*b*) A. Kirschning, W. Solodenko and K. Mennecke, *Chem. – Eur. J.*, 2006, **12**, 5972–5990.
39 G. J. Janz and S. C. Wait, *J. Chem. Phys.*, 1955, **23**, 1550– 1551.